CHAPTER 4

Numerical study of flow and thermal characteristics of turbulent jet on isothermal wavy wall

4.1 Introduction

In the present work, low Reynolds number $k-\epsilon$ RNG model is used to study the hydraulic and thermal characteristics of turbulent wall jet on the wavy wall. The sinusoidal profile ($y = A * sin(\omega_N x)$) is used for the wavy wall, where $\omega_N = 2\pi N/L$ is the frequency with suffix N denoting the number of cycles for the given length L and A is the amplitude. The influence of amplitude and frequency of the wavy wall has been studied to get an optimum amplitude and frequency for maximum heat transfer rate. For this, the amplitude is varied from 0.0 to 0.8 and frequency is varied from ω_4 to ω_{12}; the suffix 4 and 12 shows number of cycles for a given length L=1500mm, and the wall is maintained at a constant temperature of 300K. At the inlet, the Reynolds number is kept constant (15000) for all the cases, which is achieved by a uniform velocity of 10.95 m/s produced by the slotted nozzle of height 20 mm. The flow and heat transfer characteristics in the viscous sub layer of wavy wall of different frequencies have been studied for the first time. The influence of amplitude and frequency on the separation and % of total area under re-circulation zone have also been discussed, which have vital role in understanding the heat transfer phenomena near the wavy wall.

4.2 Results and discussion

4.2.1 Influence of amplitude for frequency, ω_{10}

To study the influence of amplitude on the flow and heat transfer characteristics of turbulent wall jet on wavy wall the frequency is fixed to ω_{10} and the amplitude is varied from 0.0 to 0.8 and the results are compared with the results of the plane wall case.

4.2.1.1 Streamwise flow evolution

It is well known that the streamwise flow development is sensitive to various parameters like, inlet conditions, flow domain, and the surface on which flow occurs. The influence of inlet conditions on the flow development has been studied by many researchers on the basis of Reynolds number, the shape of exit profile, nozzle geometry and using co flow. Apart from that, other influencing parameter like the shape of wall has gained very less attention. In order to explain the effect of wavy surface on flow evolution, the streamwise mean flow development of turbulent wall jet has been studied. It has been done with the help of streamwise mean velocity contour, streamwise variation of jet half width, $Y_{0.5}$, inner boundary layer Y_{max} and local maximum streamwise velocity, U_{max}.

Fig. 4.1 shows the streamwise mean velocity contour for the wavy wall jet for the amplitudes 0.2, 0.4, 0.6 and 0.8. The contour reveals that as the amplitude increases the velocity near crest increases and the jet spread also increases. The trend of free shear layer also becomes wavy for the wavy wall and as the amplitude increases, the waviness of free shear also increases for initial cycles. To explain the growth of jet spread, the growth of inner shear layer, the growth of outer shear layer and the decay of local maximum streamwise velocity, graph of $Y_{0.5}$, Y_{max}, $(Y_{0.5} - Y_{max})$ and U_{max} are shown in figs. 5.13b - 5.13a respectively. The jet half width $Y_{0.5}$ is the distance in cross streamwise direction from the wall in outer shear layer where the local mean streamwise velocity becomes half of U_{max} and Y_{max} is the distance of local maximum streamwise velocity. Fig. 5.13b shows the growth of jet spread of a plane wall jet and wavy wall jet with different amplitudes. The results of Schneider and Goldstein [86], Abrahamsson et al. [3], Banyassady and Piomelli [13] and Naqavi et al. [67] are also included for the comparison. They examined the plane wall jet for a Reynolds number of 14000 [86], 15000 [3] and 7500 [13, 67]. A good match can be seen with the experimental data of [86] up to $X = 40$ and after that a little deviation is noticed. Apart from this, a fair agreement with [3], [13], and [67] can be seen for the present plane wall data. From fig. 5.13b, it can be analysed that the trend of jet spread becomes wavy for wavy surface where maxima on the graph shows $Y_{0.5}$ at the trough of the

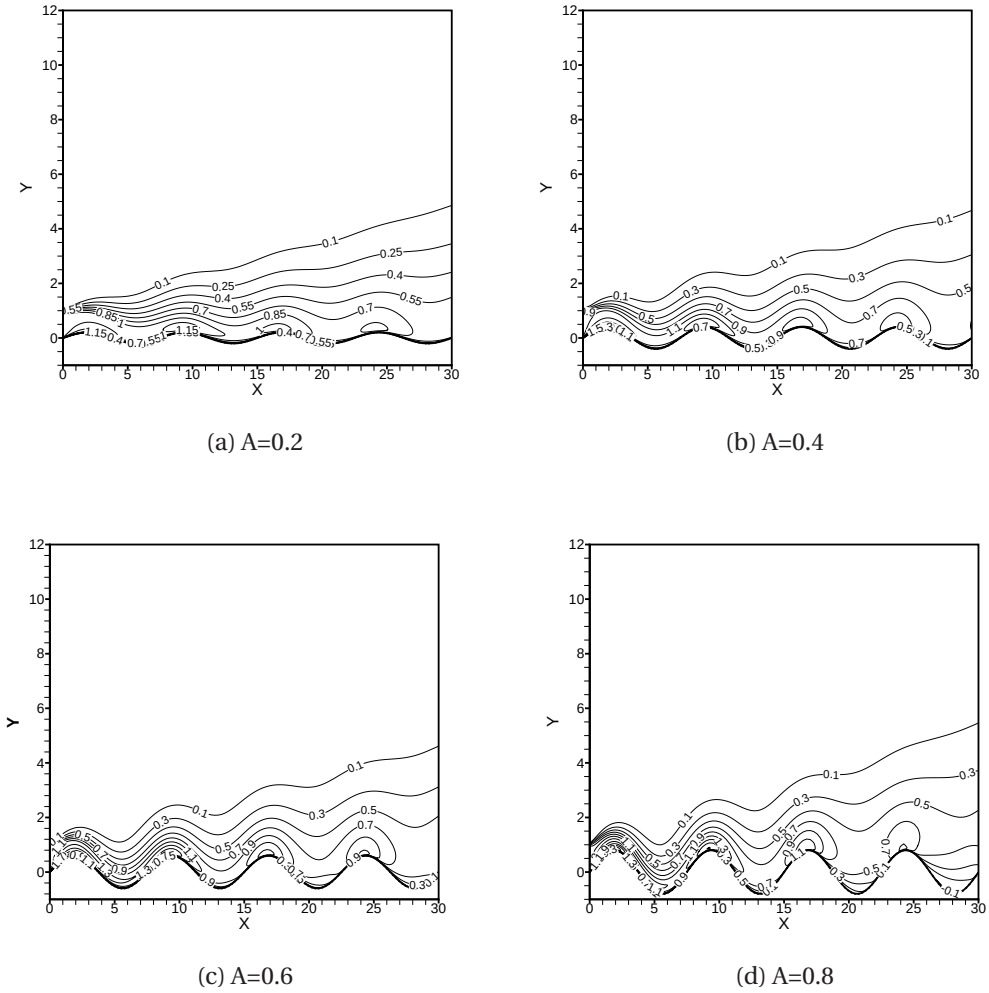

(a) A=0.2

(b) A=0.4

(c) A=0.6

(d) A=0.8

Figure 4.1: Streamwise mean velocity contour for different amplitudes

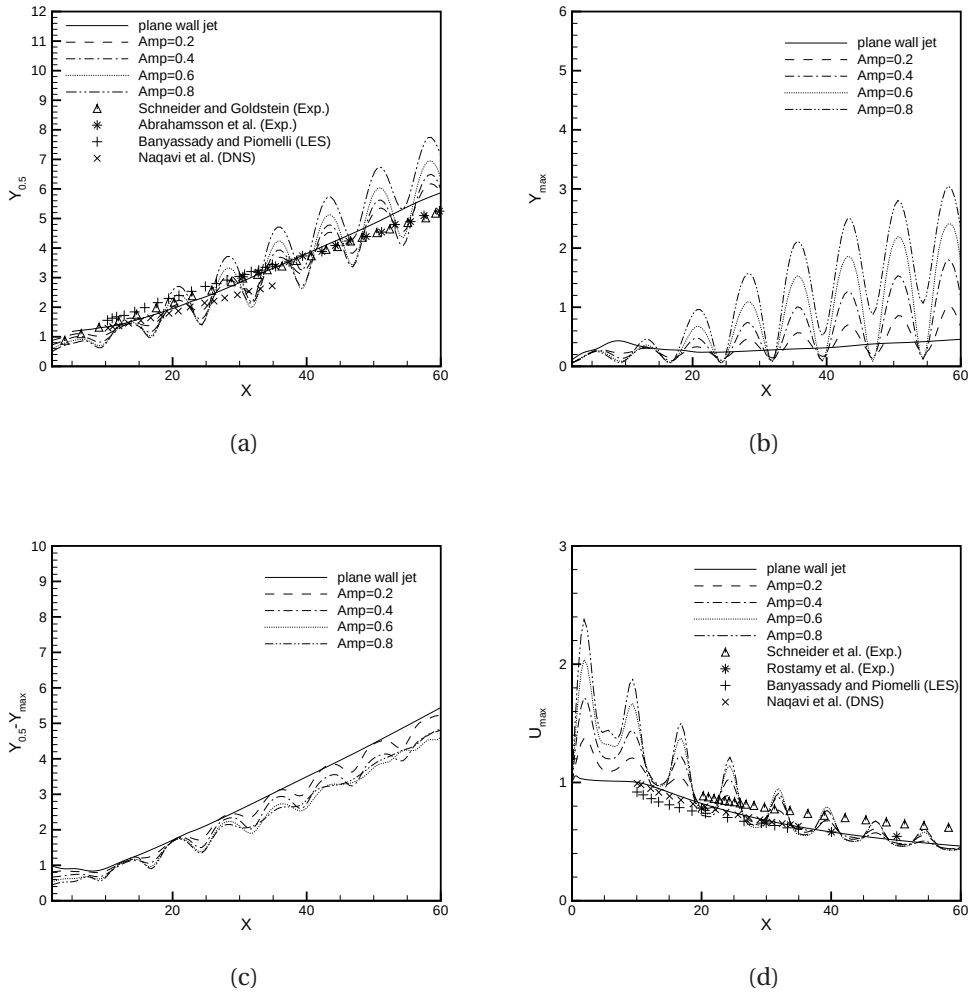

Figure 4.2: The variation in the (a) growth of jet spread, (b) growth of outer shear layer, (c) growth of inner shear layer and (d) decay of maximum local streamwise velocity along the wavy surface of different amplitudes and comparison with the result available in the literature for plane wall jet.

wall and minima shows $Y_{0.5}$ at the crest. This means that jet spread is highest at trough and lowest at crest of every cycle. The reason behind this is the acceleration of the fluid near the crest (fig. 5.13a) and to satisfy the continuity equation jet spread decreases and becomes minimum at the crest. As fluid leaves the crest, it starts decelerating (fig. 5.13a) and to satisfy the continuity equation, jet spread increases and becomes maximum at trough. Fig. 5.13b also shows influence of the amplitude on the jet spread; for near field $X \leq 15$, spread rate decreases with the increase in amplitude and further downstream it increases as amplitude increases.

The growth of inner shear layer is shown in fig. 5.13c with the help of cross streamwise location of Y_{max}. The locus of Y_{max} is used to separate the inner and outer shear layers of the flow. In the case of plane wall jet, inner shear layer has very restricted growth due to the wall placed adjacent to the jet. For the plane wall jet, the inner shear layer is maximum at $X = 9$ and then it decreases till $X = 20$. The potential core is maintained till $X = 9$ (Fig.5.13a) and it gets thinner as fluid moves forward due to the viscous effect near the wall. That is why the location of U_{max} increases. At the end of potential core, transition zone starts and due to mixing of fluid, Y_{max} decreases. After that, it increases gradually with a constant rate in the developed region. This trend is not seen for the wavy wall as the potential core gets distorted initially. In the case of wavy wall, the inner shear layer growth also shows wavy trend with minima and maxima at the crest and trough of every cycle as shown in fig. 5.13c. And the growth of inner shear layer increases with increase in the amplitude of wavy wall. The influence of amplitude on outer shear layer is illustrated by $Y_{0.5} - Y_{max}$ in fig. 5.13d. As the amplitude of wavy wall increases the growth of outer shear layer decreases. This happens because the outer shear layer thickness $(Y_{0.5} - Y_{max})$ is obtained by subtracting inner shear layer thickness (Y_{max}) from the jet spread $(Y_{0.5})$. From figs. 5.13c and 5.13d it can be observed that for increasing amplitude of wavy wall, the increment in inner shear layer is higher than the increment in jet spread; so, outer shear layer gets compressed.

The decay of maximum local streamwise velocity, U_{max}, has been compared with the results of plane wall jet, available in the literature [13, 67, 83, 86] in fig 5.13a. It can be seen that the decay of U_{max} for plane wall jet has a very good agreement with the result of [67] and [82] and also gives fair agreement with the rest of the two ([86] and [13]). In the case of wavy wall, the potential core gets distorted as soon as the jet comes in contact with the wall and attains a maximum value at the first crest location. At the first crest location $X = 1.875$, U_{max} value increases by 37%, 71%, 103% and 137% for the amplitudes 0.2, 0.4, 0.6 and 0.8 respectively in comparison to the plane wall jet. The influence of amplitude on the decay of maximum streamwise velocity is high in near field $X \leq 25$. It can also be

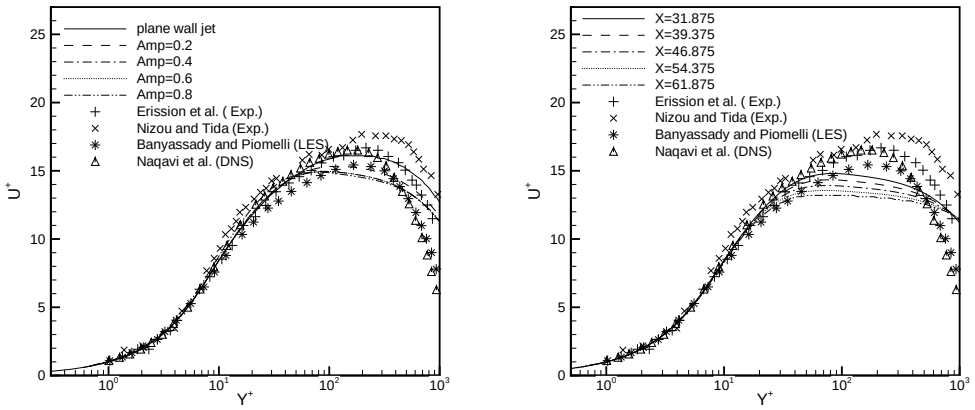

(a) (b)

Figure 4.3: Comparison of inner region velocity profile (a) for all cases at $X = 31.875$, (b) for different crest locations on wavy wall with amplitude 0.5.

observed from fig. 5.13a that for all the cases, the decay rate at the crest is higher than the decay rate at the trough in downstream direction.

4.2.1.2 Velocity profile in inner region ($u^+ - y^+$)

The flow behavior near the wall is a complex phenomenon and to get a clear understanding, the concept of u^+ and y^+ has come in existence. The u^+ and y^+ are nondimensional velocity and cross stream position from the wall obtained by the inner scaling technique, as discussed by Wygnansky et al. [103]. The $u^+$is given by u/u_*, where u_* is the friction velocity ($u_* = \sqrt{\frac{\tau_\omega}{\rho}}$) and y^+ is given by $(yu_*)/\nu$ where ν is the kinematic viscosity. The near wall velocity profile is divided in three regions: first region is laminar sublayer, $y^+ \leq 5$, where viscous shear dominates and u^+ follows linear relation with y^+ ($u^+ = y^+$). The second is log-law region, $30 \leq y^+ \leq 200$, where turbulent and viscous effects are equally important and u^+ follows logarithmic relation with y^+, $u^+ = A\,ln(y^+) + B$, where A and B are constants. The third one is the buffer layer, $5 \leq y^+ \leq 30$, which is in between the viscous sublayer and log-law region and does not follow any specific trend. Figs. 4.3a and 4.3b show the comparison of flow behavior near the wall region for the studied cases and at different crest locations of 0.5 amplitude, respectively. The present results are compared with the results available in the literature ([25], [71],[13] and [67]). In fig. 4.3a, the velocity profile for all the cases overlaps with the literature data in viscous sublayer and buffer layer. But, in the log law region, deviation starts. This means that present simulation result follows the universal law of wall relationship, $u^+ = y^+$. In the log-law region, plane wall jet

Table 4.1: Logarithmic equation constants of inner velocity profiles for different amplitudes at location $X = 31.875$.

Amplitude	A	B	R^2 (goodness if fit)	Range
0.0	2.31	5.3	0.99	$30 \leq y^+ \leq 90$
0.2	1.55	8.47	0.96	$35 \leq y^+ \leq 90$
0.4	1.20	9.76	0.95	$40 \leq y^+ \leq 80$
0.6	0.98	10.82	0.96	$30 \leq y^+ \leq 90$
0.8	0.98	10.82	0.96	$30 \leq y^+ \leq 90$

profile follows the equation $u^+ = Alog(y^+) + B$, where $A = 2.31$ and $B = 5.3$. The current value is close to the value given by Naqavi et al. [67] ($A = 2.5$ and $B = 5.2$) and Eriksson et al. [25] ($A = 2.44$ and $B = 5.0$). In the log-law region, as the amplitude of wavy wall increases, the velocity profile goes down in comparison to the plane wall jet and the value of constants A and B vary as listed in table 4.1. From table 4.1, it can be observed that the range of log-law region becomes shorter as the amplitude of wavy surface increases from plane wall to 0.8. Fig. 4.3b represents the velocity profile in inner region at the crest of wavy wall for amplitude 0.5. This can be seen that the profile remains unaffected in the viscous sublayer. In log law region and outer region the magnitude of u^+starts decreasing with the downstream location.

4.2.1.3 Temperature profile in inner region ($T^+ - y^+$)

Similar to the flow field, the temperature profile near the wall is explained with the help of T^+ and y^+ plots. Here, T^+ is the dimensionless temperature given by $\frac{T_w - T}{T_*}$, where T_w is wall temperature, T is the temperature of fluid and $T_* = \frac{q_w}{\rho C_p u_*}$ is the friction temperature. The temperature profile in this region has been further divided in same manner as the velocity profile. The empirical relation followed by temperature profile in laminar sublayer and in log law region are $T^+ = Pr\, y^+$ and $T^+ = A\, ln(y^+) + B$ respectively. The behavior of temperature profile near the wall region has been illustrated in fig. 4.4. The present computational results have been compared with the result of [67] and [70]. Fig. 4.4a shows the temperature profiles of all the cases at $X = 31.875$ and the listed literature data. It can be seen that they follow the linear relation $T^+ = Pr\, y^+$ in viscous sublayer. For all the present data, the linear relation is valid maximum up to $y^+ = 7$ which is exactly same as the Nizou's [70] observation. In log law region, deviation between the literature data and the present plane wall jet can be noticed. This may be because of, they have used heated wall in spite of heated jet, which leads to different profile in log law and outer region. In the log law region ($30 \leq y^+ \leq 90$), plane wall follows the logarithmic equation $T^+ = A\, ln(y^+) + B$,

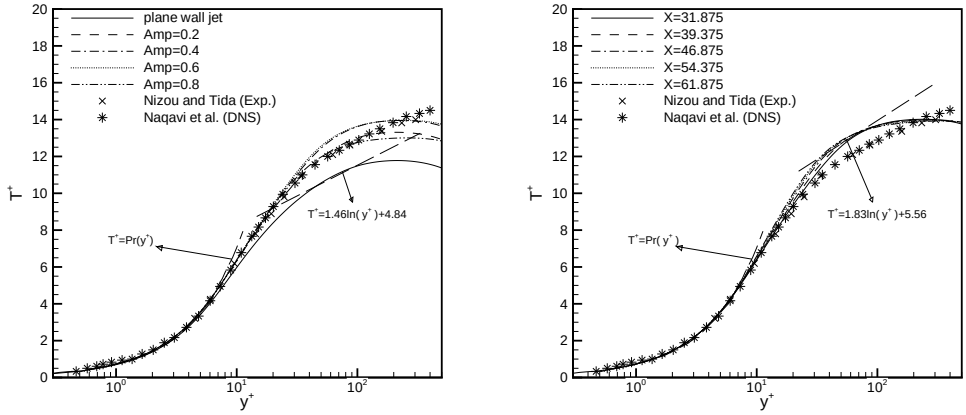

(a) (b)

Figure 4.4: Comparison of inner region temperature profile (a) for all cases at $X = 31.875$, (b) for different crest locations on wavy wall with amplitude 0.5.

Table 4.2: Logarithmic equation constants of Temperature profiles for different amplitudes at location $X = 31.875$.

Amplitude	A	B	R^2 (goodness if fit)
0.2	2.31	2.70	0.978
0.4	2.42	2.86	0.975
0.6	2.35	3.15	0.970
0.8	1.83	4.60	0.960

where $A = 1.86$ and $B = 3.14$, which are closer to the result $A = 2.08$ and $B = 3.5$ given by Naqavi et al. [67]. As the amplitude of wavy wall increases, the temperature profile moves upward in log law region up to 0.6 amplitude and thereafter it goes down. The constants for logarithmic equation for the wavy walls are mentioned in table 4.2 for the range of $30 \leq y^+ \leq 90$. Fig. 4.4b shows the variation in temperature profile at the different crest positions in streamwise direction for amplitude 0.5. The temperature profile curves for all the locations are almost same with a small variation in the log law and outer regions.

4.2.1.4 Mass Entrainment

The entrainment of ambient fluid starts as soon as the jet comes out of the nozzle due to the discontinuity of velocity between the jet and the ambient fluid. The rate of entrainment depends on the initial momentum of the jet at inlet and the magnitude of velocity discontinuity with the ambient fluid. Fig. 4.5a presents the variation of Q/Q_0 with the X, where $Q = \Delta_{y_1}^{\infty} U\,dy$ stands for the rate of flow per unit area at any jet section. The flow

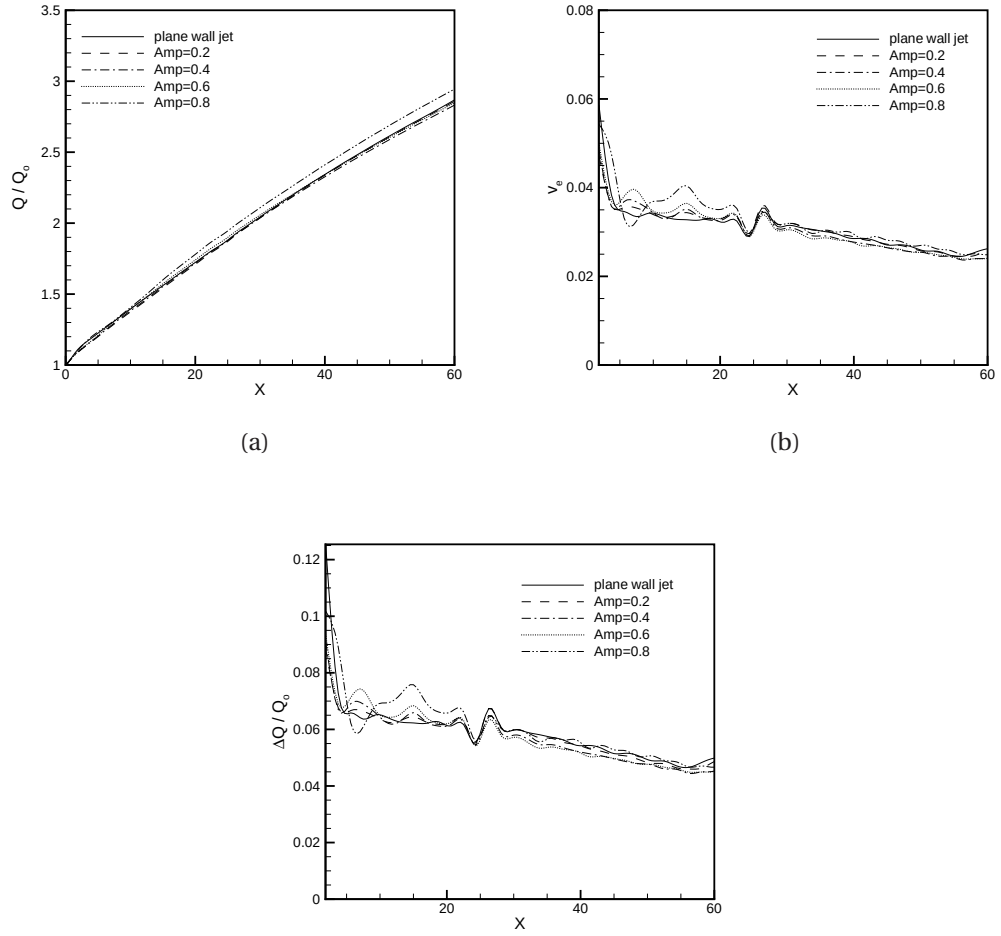

Figure 4.5: Variation in normalized (a) Volume flow rate, (b) entrainment velocity and (c) entrainment volume along the flow for different amplitudes

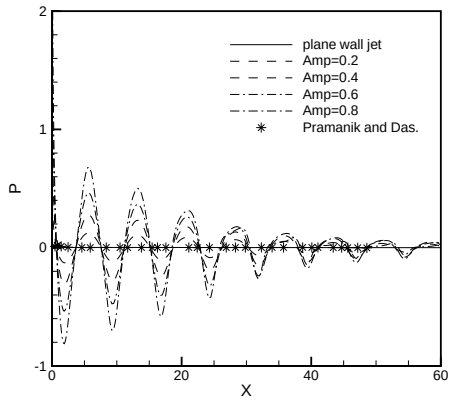

Figure 4.6: Comparison of steady wall pressure for all the cases

rate Q is normalized by the flow rate at the nozzle exit Q_0. From fig. 4.5a, it can be seen that the flow rate increases with increase in X, indicating the entrainment of the surrounding fluid. The entrainment is almost linear with X. It can be noticed that the entrainment is hardly influenced by the waviness of the wall. A marginal increase can be seen for amplitude 0.8. The entrainment velocity, v_e, is obtained by differentiating the volume flow rate Q with respect to longitudinal distance X, i.e $v_e = \frac{dQ}{dX} = \frac{d}{dx}(\Delta_{y_x}^{\infty} U dy)$ [75]. The variation of v_e for all the cases is shown in fig. 4.5b, where it can be seen that entrainment is maximum just after the nozzle exit and then decreases sharply till $X = 5$; beyond that, entrainment decays with a slow rate. The entrainment velocity is fluctuating up to $X = 30$ and after that it decays with a constant rate. This happens because of the transitional zone till $X = 30$; flow is still developing in this region. Once the flow develops, the entrainment rate is constant. In fig. 4.5c, the variation of volume flow rate entrainment for plane wall wavy wall jets shows same trend as shown in fig. 4.5b for the entrainment velocity. The entrainment of volume flow rate $\triangle Q$ is obtained by subtracting the integrated volume flow rate from two consecutive vertical lines on which Q is calculated. The distance between the two consecutive lines, dx, remains constant through the flow domain.

4.2.1.5 Pressure at the wall

Fig. 4.6 shows variation of static pressure at the wall for the wavy walls of amplitude 0.2 to 0.8. The result of plane wall is compared with the result of Pramanik and Das [74]. It can be seen that in the case of plane wall, pressure remains almost constant ($P = 0$) throughout the wall length, except for a very small distance near the nozzle exit. For wavy surfaces, the pressure at the wall is fluctuating from maximum to minimum for each cycle. At the exit of nozzle, pressure is maximum and it starts decreasing at a very high rate and be-

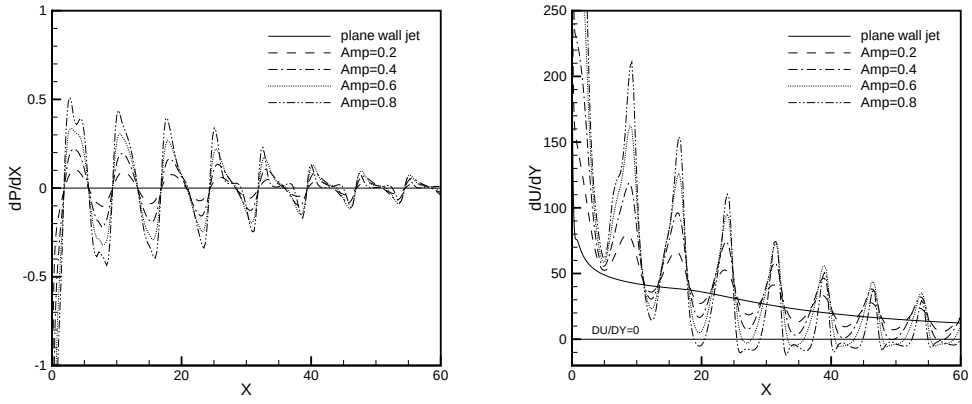

(a) (b)

Figure 4.7: Variation of (a) pressure gradient and (b) velocity gradient at the wall for different amplitude wavy walls

comes minimum at $X = 1.875$ (first crest) and after this location, pressure at the wall starts increasing and attains maximum value at $X = 5.625$ (first trough). In a similar manner, pressure at the wall is minimum at the crest and maximum at the trough for each cycle of the wavy wall. The trend of pressure at wall is just opposite to the trend of U_{max} because of the conversion of pressure energy into kinetic energy as the flow takes place from nozzle exit to the crest and vice-versa at the trough. The magnitude of pressure at wall increases as amplitude of wavy wall increases from 0.2 to 0.8. The effect of waviness of wall on static wall pressure reduces with increase in X and it approaches to plane wall case.

4.2.1.6 Flow Separation

The flow gets separated from the wall when the flow travels through adverse pressure gradient (dP/dX≥0). The separation starts from the point where the velocity gradient (dU/dY) becomes zero at the wall. Figs. 4.7a and 4.7b are the plots of normalized pressure gradient, dP/dX and normalized velocity gradient, dU/dY at the wall, respectively. The fig. 4.7a shows that the region from the crest to trough of every cycle on wavy wall faces the adverse pressure gradient. The pressure gradient remains zero in the case of plane wall and at all the crests and troughs in the case of wavy wall. The magnitude of pressure gradient increases as the amplitude of wavy wall increases. Fig. 4.7b shows the separation point and re-circulation region for wavy walls. In spite of adverse pressure gradient, the flow remains attached throughout the flow for wavy surface up to 0.3 amplitude, because of the low intensity of the adverse pressure gradient. As the amplitude increases from 0.4

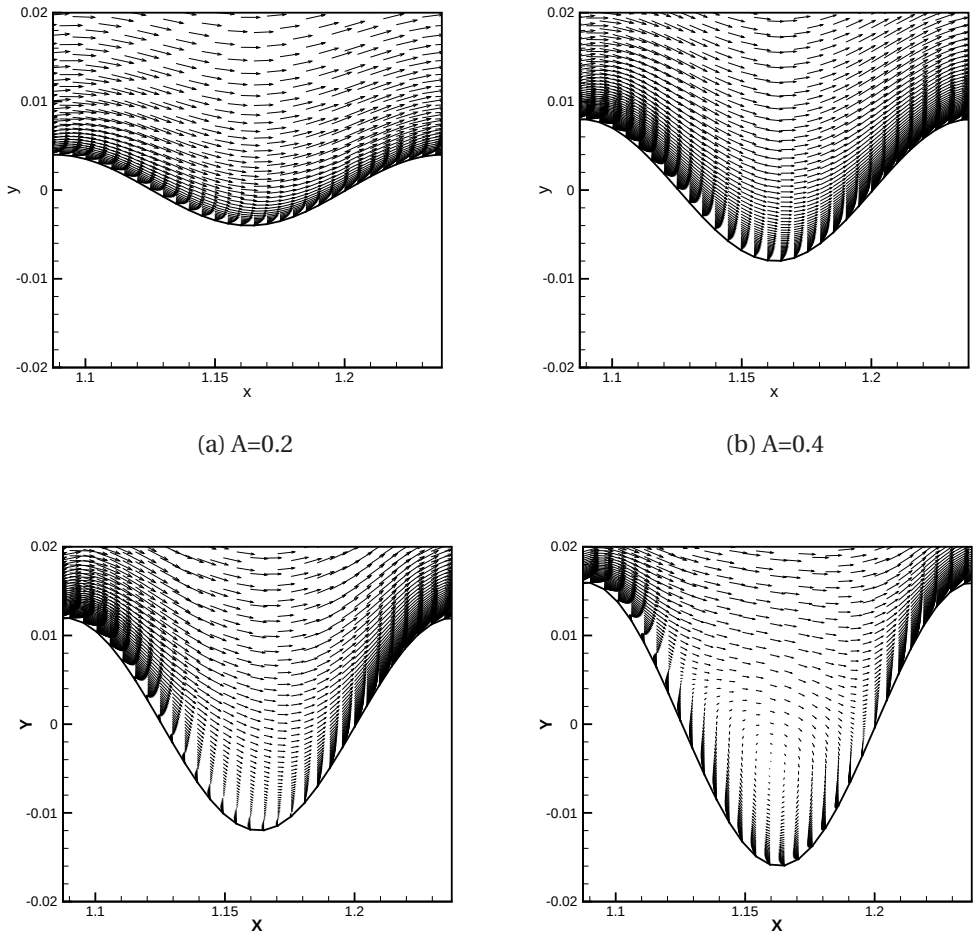

(a) A=0.2

(b) A=0.4

(c) A=0.6

(d) A=0.8

Figure 4.8: The velocity vector contour near the 8^{th} trough region for different amplitudes

to 0.8 the flow separation starts early, i.e for amplitude 0.4, 0.5, 0.6, 0.7 and 0.8, separation takes place at $X = 56.4$, $X = 41.0$, $X = 26.3$, $X = 25.9$ and $X = 25.5$, which are at 8^{th}, 6^{th}, 4^{th}, 4^{th}, 4^{th}crest to trough region. The region where dU/dY curves are below the zero line shows the recirculation zone and for higher amplitude, the area of recirculation zone increases. The velocity vector near the 8^{th} trough for the various amplitudes is shown in fig. 4.8. It can be seen that the flow remains attached to the surface for amplitude 0.2. A small recirculation zone with low intensity is noticed for amplitude 0.4 (not visible in fig. 4.8b). For the amplitudes 0.6 and 0.8, the re-circulation zone is clearly visible and the intensity of re-circulation is higher for the higher amplitude. It indicates that the intensity of re-circulation increases with increase in the amplitude of the wavy wall. The reason is quite obvious; increase in amplitude increases the slope of the wall which supports the favor-

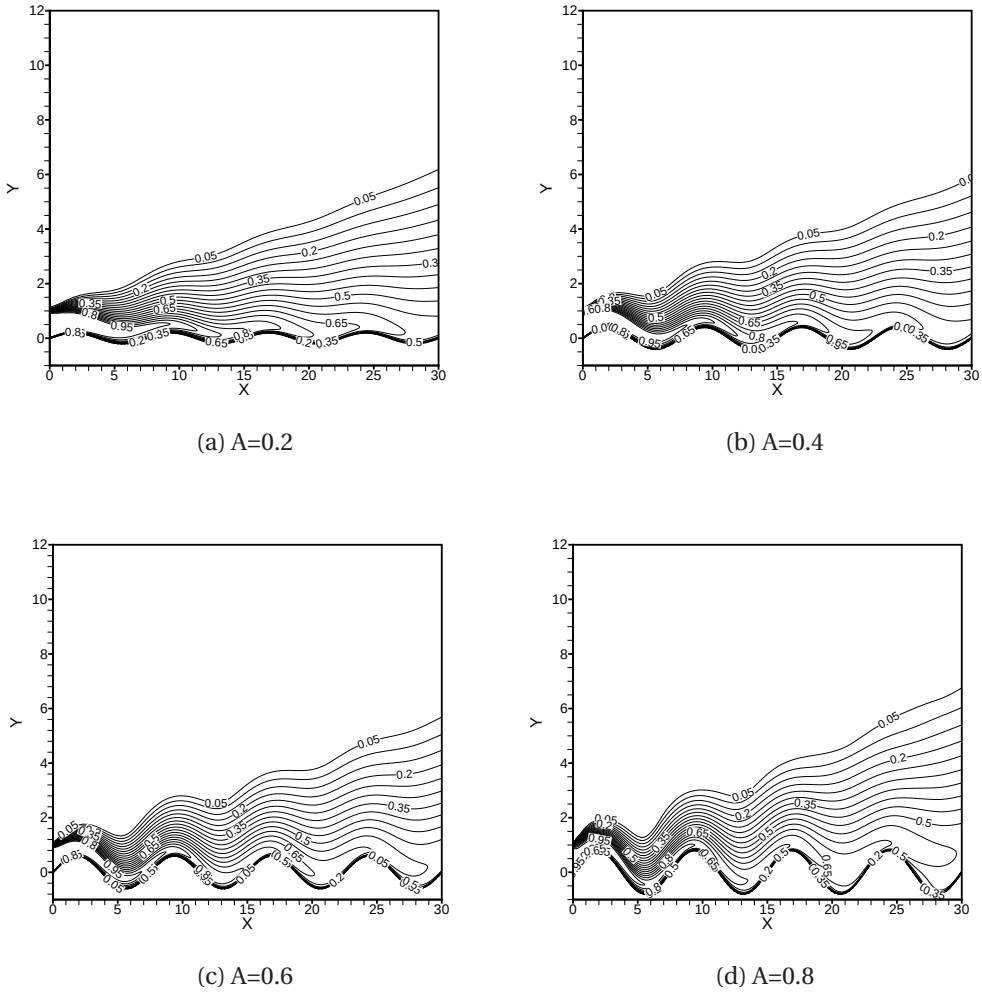

(a) A=0.2

(b) A=0.4

(c) A=0.6

(d) A=0.8

Figure 4.9: Temperature contour for different amplitudes

able condition of flow separation. It is also worth noticing that the point of flow separation shifts towards the crest with increase in the amplitude of the wall.

4.2.1.7 Temperature variation along the plate

The temperature contour for amplitudes 0.2, 0.4, 0.6 and 0.8 is shown in fig. 4.9. The contour shows that the thermal potential core becomes shorter and thinner as the amplitude increases. This is due to the intense mixing of jet's fluid with the quiscent fluid. Fig. 4.10 shows the thermal characteristics of jet of the studied cases. The decay of local maximum temperature of jet θ_{max} and development of thermal wall boundary layer thickness Y_{Tmax} are shown in figures 4.10a and 4.10b respectively, where $\theta_{max} = (T_{max} - T_\infty)/(T_0 - T_\infty)$, is the normalized local maximum temperature, Y_{Tmax} is the cross-stream distance from

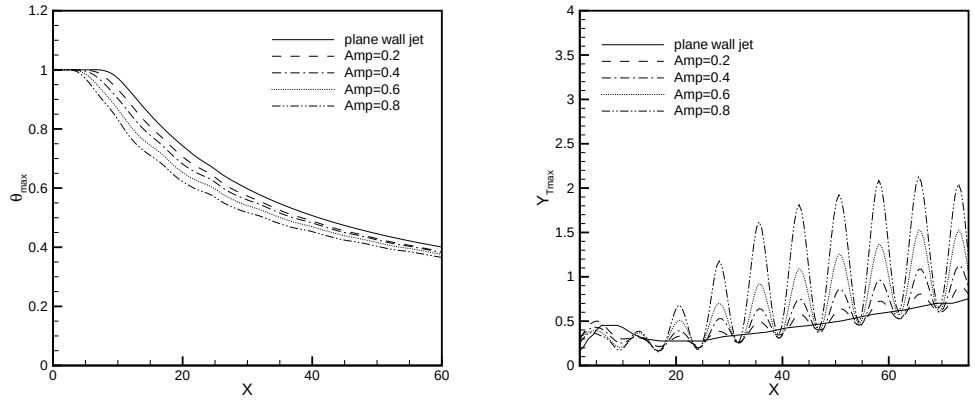

(a) (b)

Figure 4.10: The comparison of (a) decay of maximum local temperature and (b) growth of thermal wall boundary layer thickness

the wall where temperature θ_{max} is achieved. From fig. 4.10a, it can be observed that the length of the thermal potential core decreases from $X = 7.5$ to $X = 3.75$ when amplitude of the wall changes from 0.0 to 0.8. Also, the decay rate of maximum temperature increases as amplitude increases. The reduction in thermal potential core with increase in the amplitude is dictated by higher heat transfer rate. Growth of thermal wall boundary layer Y_{Tmax} is illustrated in fig. 4.10b. At the trough, Y_{Tmax} increases as the amplitude of wavy wall increases and at the crest, Y_{Tmax} changes marginally. The trend of Y_{Tmax} is similar to the trend of growth of inner shear layer Y_{max}, as shown in fig. 5.13c.

4.2.1.8 Variation in local Nusselt number

The variation of local Nusselt number along the plane and wavy wall is explained in fig. 4.11. The local Nusselt number Nu_x is calculated by the following equation, where Q_w is the wall heat flux:

$$Nu_x = (Q_w PrRe)/(\rho C_p U_0 (T_0 - T_\infty))$$

Fig. 4.11 shows that for all the cases, the Nu_x is maximum near the nozzle exit. The Nu_x decreases slowly in the downstream direction in the case of plane wall jet. For wavy walls the decay of Nu_x follows wavy pattern, i.e. for each cycle trend shows one maximum and one minimum value that keeps on decreasing with increase in X. In near flow field, up to $X = 19$, the Nusselt number increases as the amplitude of wavy wall increases. The

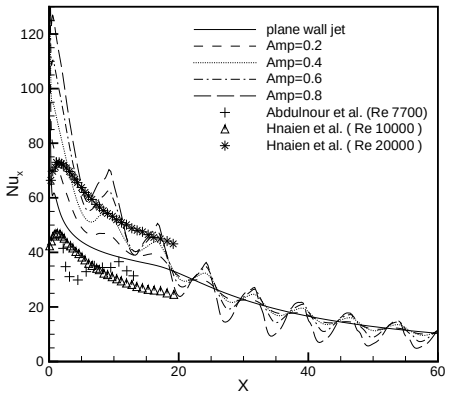

Figure 4.11: Variation of local Nusselt number along the wall of different amplitudes and comparison with the plane wall results available in the literature

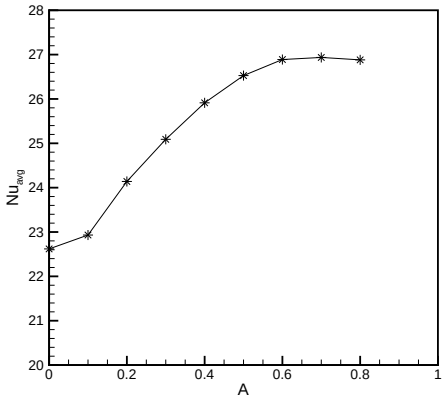

Figure 4.12: Variation of average Nusselt number for different amplitude wavy walls

effect of wavy wall on local Nusselt number decreases with increase in X. The average Nusselt number is calculated by integrating the local Nusselt number throughout the bottom wall and is defined as $Nu_{avg} = \Delta_0^S Nu_x ds$. Fig. 4.12 shows the variation of average Nusselt number, Nu_{avg} against the amplitude of wavy wall. The average Nusselt number for the wavy wall increases as the amplitude of wavy wall increases up to the amplitude 0.7 and after that the Nu_{avg} decreases. Even after increase in the surface area and local maximum streamwise velocity, the heat transfer reduces for the case of 0.8 amplitude. This happens due to the increase in re-circulation zone with increasing amplitude of wavy wall. It can also be noted that there is a maximum increment in heat transfer of 19.08% for 0.7 amplitude with respect to the plane wall case.

4.2.1.9 Thermal hydraulic performance

To calculate the thermal hydraulic performance (THP), the enhancement of heat transfer and frictional loss are taken into consideration for comparison of wavy wall jet with the plane wall jet. The expression can be written as [37]

$$\text{THP} = (Nu/Nu_0)/(f/f_0)^{1/3}$$

and

$$f_x = 8\tau_w/\rho U^2$$

where f_x is Darcy Weisbach friction factor, τ_w is shear stress at the wall and U is the mean velocity at inlet. The Nu_0 and f_0 are the Nusselt number and friction factor for the plane wall jet. In the study of influence of amplitude of wavy wall on the heat transfer rate, the increment of 19.08% has been observed. On the other hand, the amplitude also affects the friction factor at the wall as shown in fig. 4.13. Fig. 4.13 shows that the friction factor is maximum near the crest and minimum near the trough. As amplitude increases, the friction factor increases in near flow region till $X \approx 10$. Beyond this, the value of friction factor increases near crest and decreases near trough for higher amplitude. Fig. 4.14 shows the trend of thermal hydraulic performance for amplitude 0.1 to 0.8. The THP of wavy wall with respect to plane wall first reduces for the first two amplitudes 0.1 and 0.2 and then it starts increasing. For the lower amplitude, the increase in friction factor is comparatively higher than the increase in heat transfer rate. The thermal hydraulic performance is improved up to 5.3% for A=0.8.

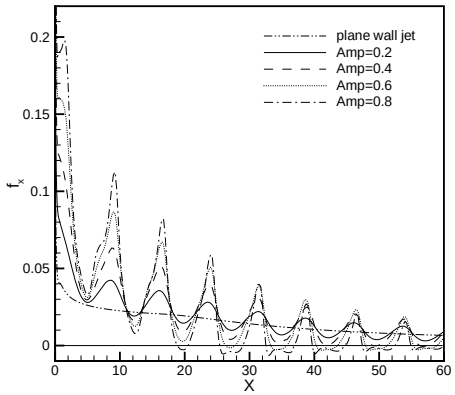

Figure 4.13: Variation of friction factor for wavy wall of different amplitudes and plane wall

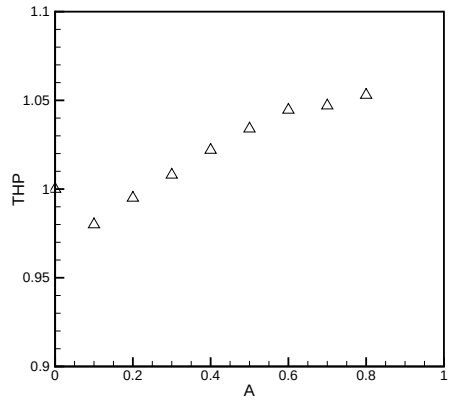

Figure 4.14: Thermal hydraulic performance for different amplitude

4.2.2 Influence of frequency $\omega_4 - \omega_{12}$

The influence of frequency has been studied on the flow and heat transfer characteristics of turbulent wall jet on wavy wall, where the frequency is varied from ω_4 to ω_{12} and the amplitude is varied from 0.0 to 0.8 , and the results are compared with the plane wall case.

4.2.2.1 Streamwise mean velocity contour

Out of many cases from amplitude 0.1 to 0.8 and frequency ω_4 to ω_{12}, for which the fluid flow and heat transfer are computed numerically, the fig. 4.15 shows the contour of streamwise mean velocity for the amplitudes 0.2, 0.4, 0.6 and 0.8 for the frequency ω_4 ,ω_8 and ω_{12}. From the contour, it can be clearly seen that for any amplitude, as the frequency increases the local streamwise velocity also increases near the crest location. It can be noted from fig. 4.15 that for the higher amplitude, the influence of the frequency becomes more intense on the streamwise velocity. This happens because, as the frequency or amplitude increases, the slope of wall also increases near the exit of the nozzle leading to higher acceleration of the fluid.

4.2.2.2 Flow development

To study the influence of frequency on the development of flow field for wavy wall jet, the trends of U_{max} and Y_{max} are discussed. The decay of U_{max} and the growth of inner shear layer (Y_{max}) are illustrated in figs. 4.16 and 4.17 respectively. The decay of U_{max} for different amplitudes is shown in figs. 4.16a, 4.16b and 4.16c for ω_4 ,ω_8 and ω_{12} frequency, respectively. For the plane wall jet, the decay of U_{max} is compared with the result of Rostamy et al. [82], Banyassady and Piomelli [13], Naqavi et al. [67] and Schneider and Goldstein [86]. The Reynolds number 14000 is taken by [86] and 7500 by [13, 67, 83]. Fig. 4.16 shows that the present result for the plane wall jet gives best match with the experimental result of Rostamy et al. [82] and DNS result of Naqavi et al. [67]. In the case of plane wall jet, the potential core is maintained till $X = 9$; just after this, the upper shear layer and lower shear layer comes in contact with each other and the transition zone starts. The jet decays with a faster rate in the transition zone as the upper shear layer and lower shear layer are in the adjusting phase. Once the upper shear layer and lower shear layer become stable with each other, the decay rate becomes constant and flow enters the developed zone. However, in the case of wavy wall, due to the undulated surface, the velocity potential core is distorted as the jet enters the flow field. As the fluid moves forward towards the first crest, the flow area reduces and to satisfy the continuity, the local streamwise velocity increases and attains its first peak. As the fluid moves from crest to trough, the flow area

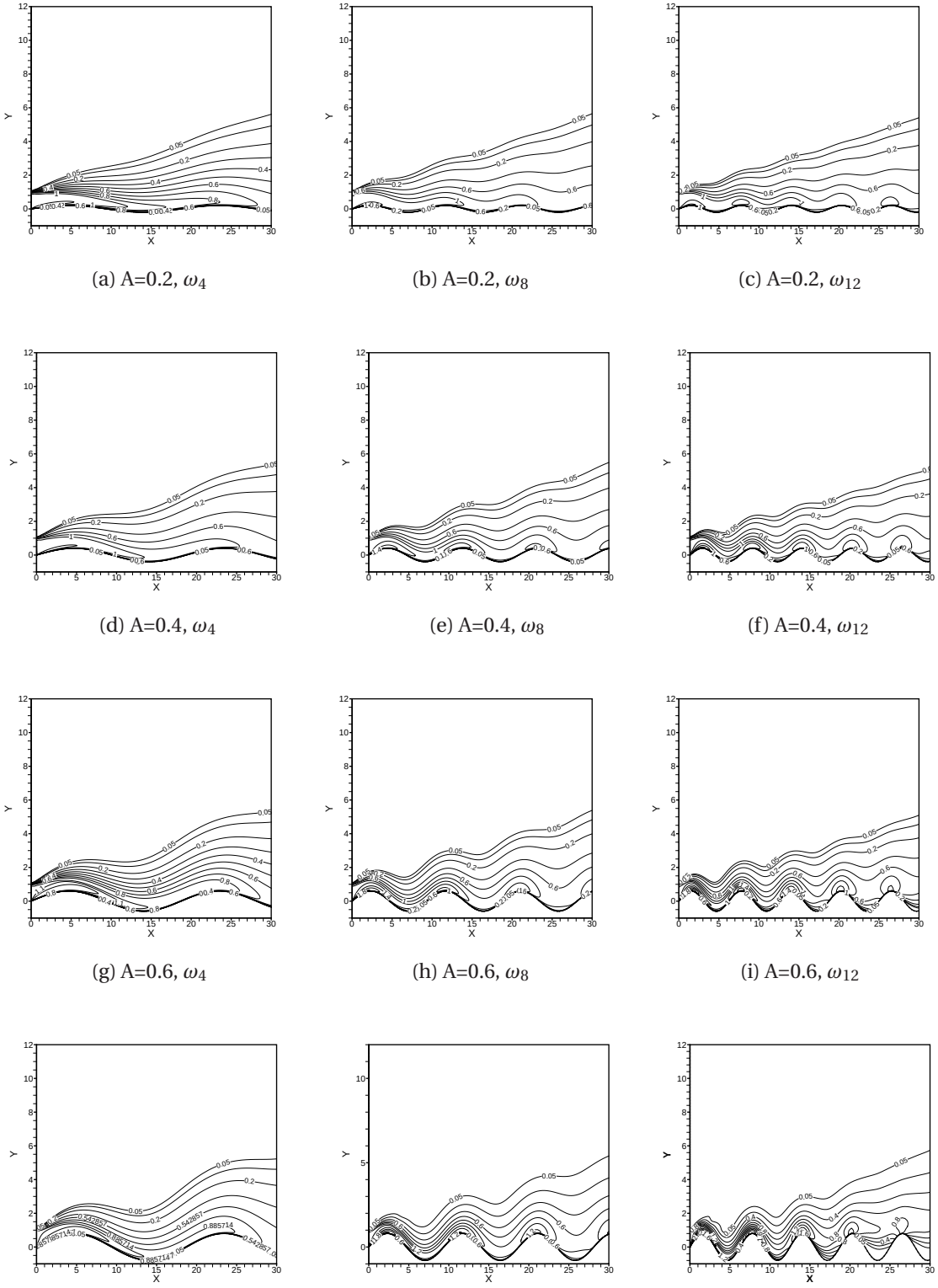

(a) A=0.2, ω_4 (b) A=0.2, ω_8 (c) A=0.2, ω_{12}

(d) A=0.4, ω_4 (e) A=0.4, ω_8 (f) A=0.4, ω_{12}

(g) A=0.6, ω_4 (h) A=0.6, ω_8 (i) A=0.6, ω_{12}

(j) A=0.8, ω_4 (k) A=0.8, ω_8 (l) A=0.8, ω_{12}

Figure 4.15: The streamwise mean velocity contour for different amplitudes and different frequencies

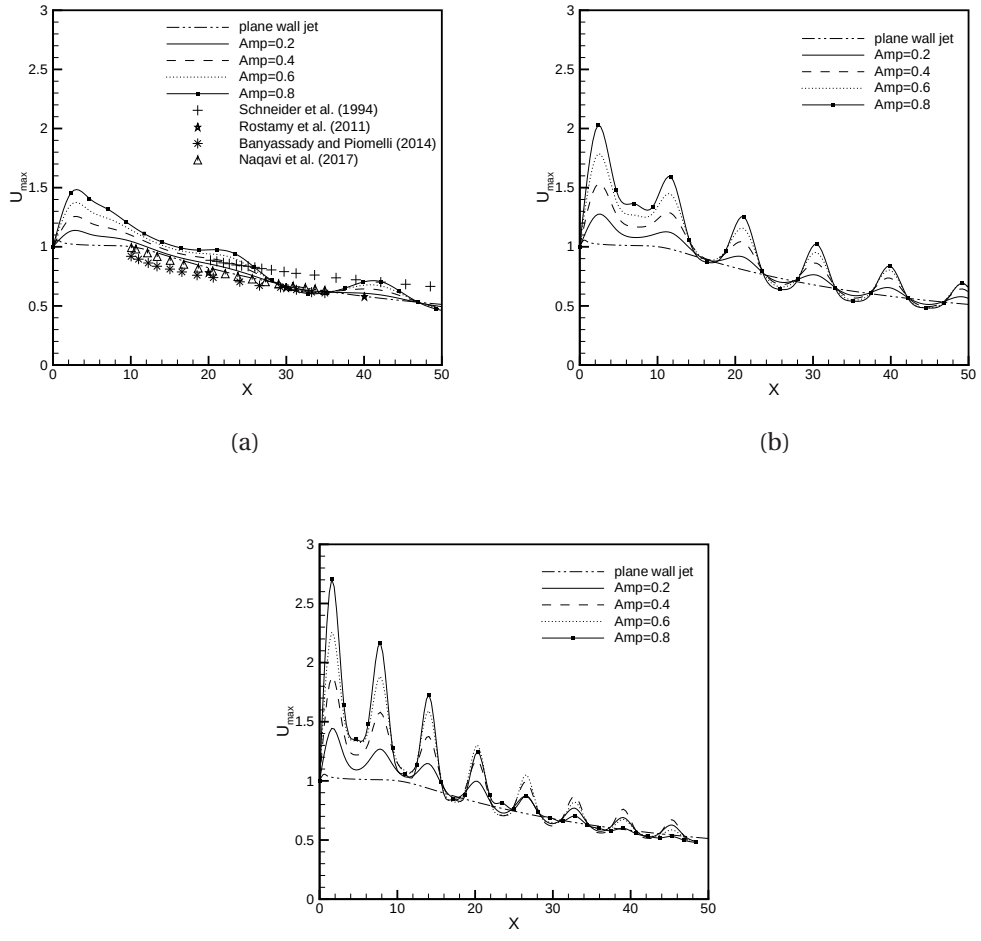

Figure 4.16: The variation of local maximum streamwise mean velocity for different amplitudes for (a) ω_4, (b) ω_8 and (c) ω_{12}

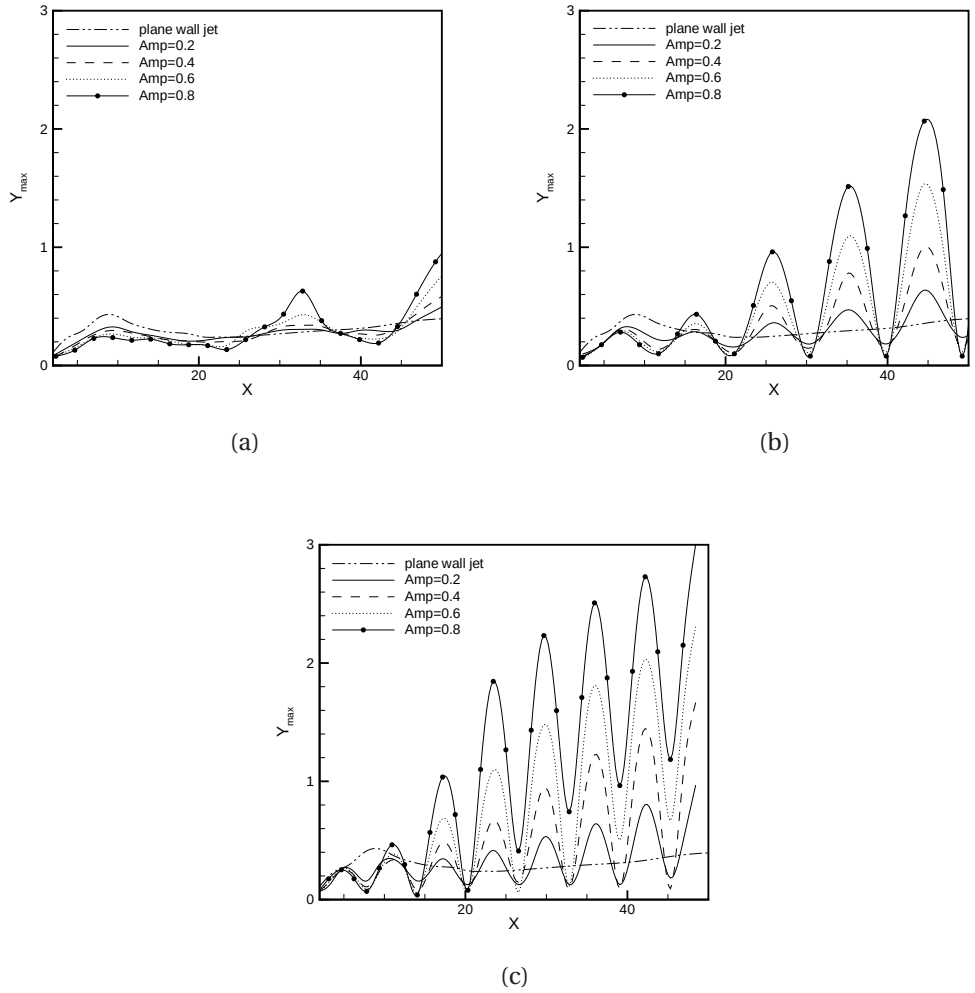

(a) (b)

(c)

Figure 4.17: The variation of inner shear layer thickness Y_{max} for different amplitudes for (a) ω_4, (b) ω_8 and (c) ω_{12}

increases and to satisfy the continuity, the flow retards itself to get minima of U_{max}. In this way, the trend of U_{max} decay for wavy wall also becomes wavy with number of maxima and minima equal to the number of cycles. In the near field, the value of U_{max} increases for the increasing amplitude and for increasing frequency. The influence of amplitude weakens as the fluid moves downstream in the far field region for ω_4 and ω_8. However, for ω_{12}, the value of U_{max} starts decreasing for higher amplitude in the far field locations. This happens due to the higher loss of kinetic energy in the case of higher frequency. The maximum increment in U_{max} with respect to the plane wall is 45.8%, 102% and 170.4% for the wavy wall frequency ω_4 , ω_8 and ω_{12} respectively , for 0.8 amplitude near the first crest.

The variation of inner shear layer thickness for ω_4, ω_8 and ω_{12} is shown in figs. 4.17a, 4.17b and 4.17c respectively, for different amplitudes. For the plane wall jet, the position

of Y_{max} remains about 0.5a till the potential core is maintained. As soon as the velocity potential core becomes exhausted, the inner shear layer starts reducing in the transition zone as the upper shear layer and lower shear layer are in the adjusting phase and the entrainment of ambient fluid tries to push the flow downward. The inner shear layer starts growing with a constant rate in the developed zone. The scenario for the wavy wall is totally different. Once fluid exits from the nozzle, the waviness of the wall obstructs the flow which increases the velocity near the wall and the position of U_{max} goes down. That is why the location of Y_{max} reduces just after the exit and reaches the minimum value near the first crest at the location of maximum U_{max}. The inner shear layer gets space to grow rapidly in the trough region, that is why Y_{max} is high in this region. From fig. 4.17, it can be seen that the influence of amplitude is very mild in the case of ω_4 in comparison to the case of ω_8 and ω_{12}. In the far field, there is an increment in the thickness of inner shear layer with the increase in the amplitude. But in the near field up to $X = 25$, $X = 14$ and $X = 10$ for ω_4 , ω_8 and ω_{12} respectively, the inner shear layer thickness reduces on increasing the amplitude. In near flow filed, the the upper shear layer and lower shear layer are in adjusting phase and by increasing the amplitude the intermixing of fluid between the two layers also increases which restricts the growth of inner shear layer.

4.2.2.3 Friction factor coefficient and separation

The friction factor coefficient on the wavy wall is an important flow parameter that reveals interesting facts about the flow behavior near the wall region. The variation of friction factor coefficient has been shown for frequencies ω_4, ω_8 and ω_{12} in figs. 4.18a, 4.18b and 4.18c respectively, for different amplitudes. The friction factor coefficient is a dimensionless quantity obtained by the normalization of wall shear stress with the inlet dynamic pressure, i.e, $f_x = 8\tau_w/\rho U^2$ [76]. The friction factor coefficient is maximum near the inlet due to the formation of high velocity gradient and the value increases with the increasing amplitude and increasing frequency. The influence of amplitude is mild for the wavy wall with frequency ω_4, and the trends are nearly similar to the plane wall jet. As the frequency increases to ω_8 and ω_{12}, the effect of amplitude becomes more dominating. The f_x maxima is located at the crest and minima at the trough because the inner shear layer is thinner near the crest with higher U_{max} value and vice versa for the trough region, which leads to higher velocity gradient in crest region in comparison to the trough region. One more important observation can be drawn from these figures that the flow gets separated from the wall when the f_x becomes zero and the zone where f_x remains negative indicates the re-circulation zone. From fig. 4.18a, it can be noted that for ω_4 flow remains attached all over the wall for all the amplitudes. For ω_8 and ω_{12}, flow starts separating from am-

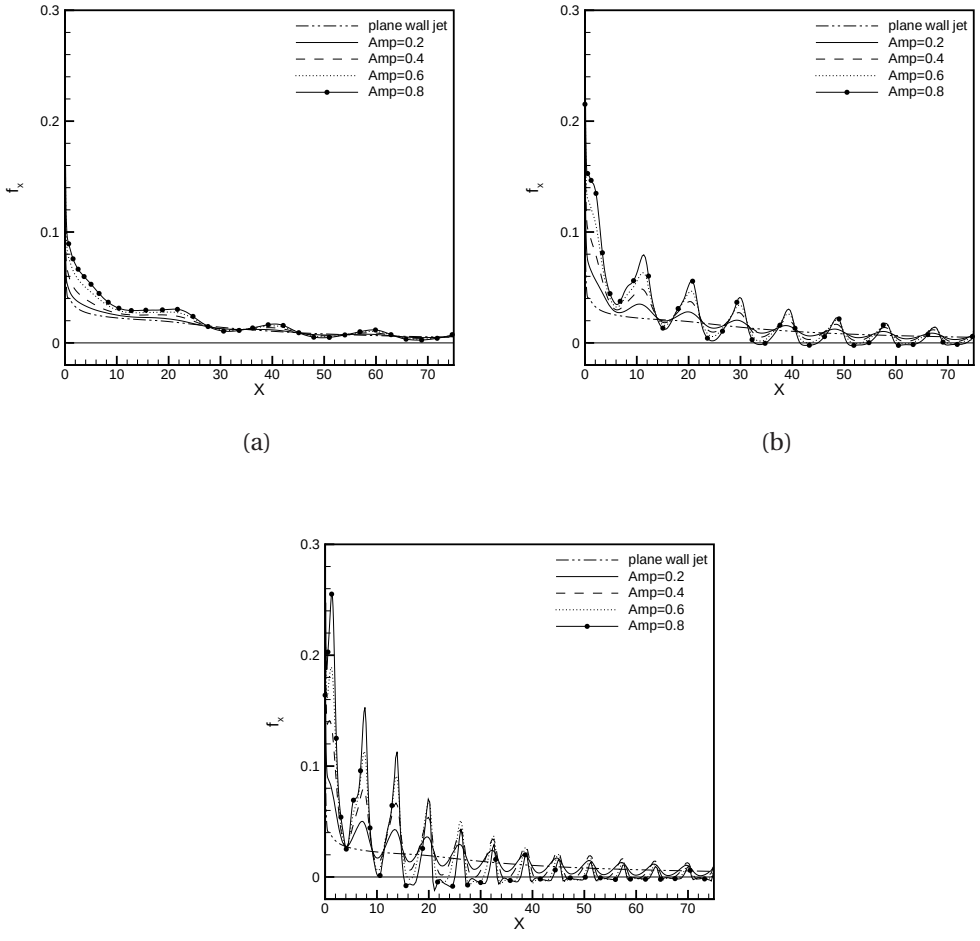

(a) (b)

(c)

Figure 4.18: The variation of friction factor coefficient on the wall for different amplitudes for (a) ω_4, (b) ω_8 and (c) ω_{12}

Table 4.3: The position in the downstream direction where the separation is initiated for first time (the % of total area under re-circulation for different cases)

$\Downarrow\omega_N \setminus$ A$\Rightarrow$	0.1	0.2	0.3	0.4	0.5	0.6	0.7	0.8
ω_4	-	-	-	-	-	-	-	-
ω_5	-	-	-	-	-	-	-	-
ω_6	-	-	-	-	-	-	-	69.0(2.0)
ω_7	-	-	-	-	-	-	48.8(6.8)	48.3(13.1)
ω_8	-	-	-	-	70.5(1.1)	43.0(8.7)	33.5(17.1)	32.8(24.7)
ω_9	-	-	-	-	46.0(9.6)	37.5(18.4)	29.0(28.1)	28.5(35.1)
ω_{10}	-	-	-	49.2(6.3)	41.0(16.3)	26.3(28.0)	25.9(36.9)	25.5(45.7)
ω_{11}	-	-	72.0(0.4)	37.6(13.3)	24.2(25.5)	23.5(36.1)	17.2(45.8)	16.7(51.2)
ω_{12}	-	-	47.4(5.6)	28.2(20.5)	21.7(32.8)	15.6(45.0)	15.5(51.5)	15.2(58.2)

plitude 0.5 and 0.3 onwards respectively. The detailed information about the location of flow separation for the first time for different amplitudes and different frequencies is listed in table 4.3. In table 4.3, the percentage of total area under the re-circulation zone is also listed inside the parenthesis in the respective column. From table 4.3, it is clear that the separation initiates early and the area under re-circulation zone increases as the amplitude or number of cycles increases. The re-circulation zone covers up to 58.2% of the total area of the wavy wall with an amplitude 0.8 and 12 cycles. For the clear visualization of the re-circulation zone, the velocity vector plot has been shown in fig. 4.19 for amplitude 0.4, 0.6 and 0.8 for wavy wall with frequency ω_4, ω_8 and ω_{12} at the 3rd, 6th and 8th trough, respectively.

4.2.2.4 Turbulent kinetic energy

Turbulent kinetic energy (TKE) is the kinetic energy associated with the eddies present in the turbulent flow. In general, the turbulent kinetic energy is defined as $k = 1/2(\overline{(u')^2} + \overline{(v')^2})$, where $\overline{(u')^2}$ and $\overline{(v')^2}$ are the variance of turbulent velocity in the streamwise and cross-stream directions, respectively; TKE signifies the intensity of turbulence in the flow. The normalised turbulent kinetic energy in cross stream direction for different amplitudes are plotted in fig. 5.16 for frequency ω_4, ω_8 and ω_{12} at the locations $X = 42.1875$ (3rd crest), $X = 39.8375$ (5th crest) and $X = 39.0625$ (7th crest), respectively. The cross stream distance $Y - Y_1$ is normalized distance from the wavy surface, where Y is the distance normal from the x-axis and Y_1 is the normal distance of wavy surface from the x-axis. It can be seen that for the same frequency, the turbulent kinetic energy increases as the amplitude increases. Two peaks can be seen in the trend of turbulent kinetic energy, the smaller one in the inner shear region and the bigger one is in the outer shear layer. And, in between

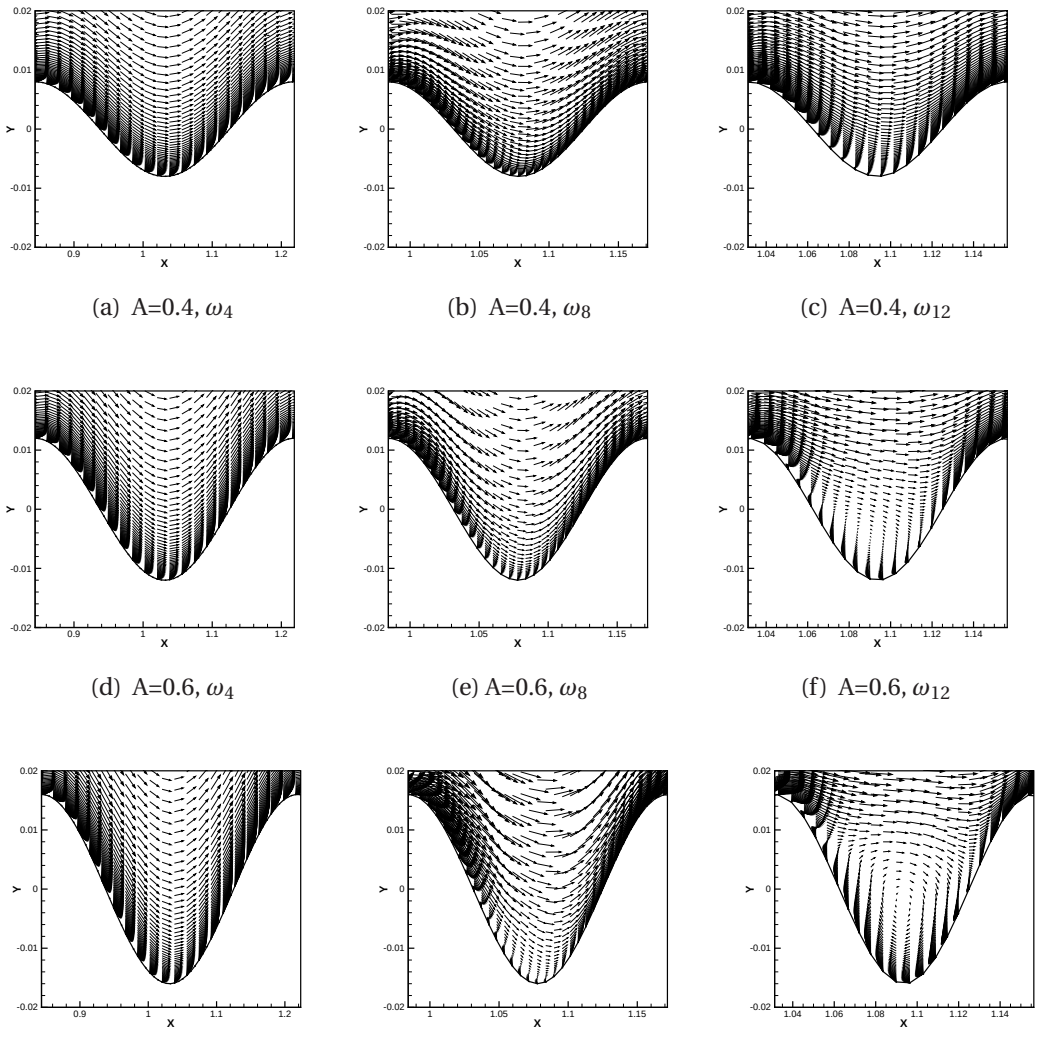

(a) A=0.4, ω_4 (b) A=0.4, ω_8 (c) A=0.4, ω_{12}

(d) A=0.6, ω_4 (e) A=0.6, ω_8 (f) A=0.6, ω_{12}

(g) A=0.8, ω_4 (h) A=0.8, ω_8 (i) A=0.8, ω_{12}

Figure 4.19: Velocity vector plot at the trough location.

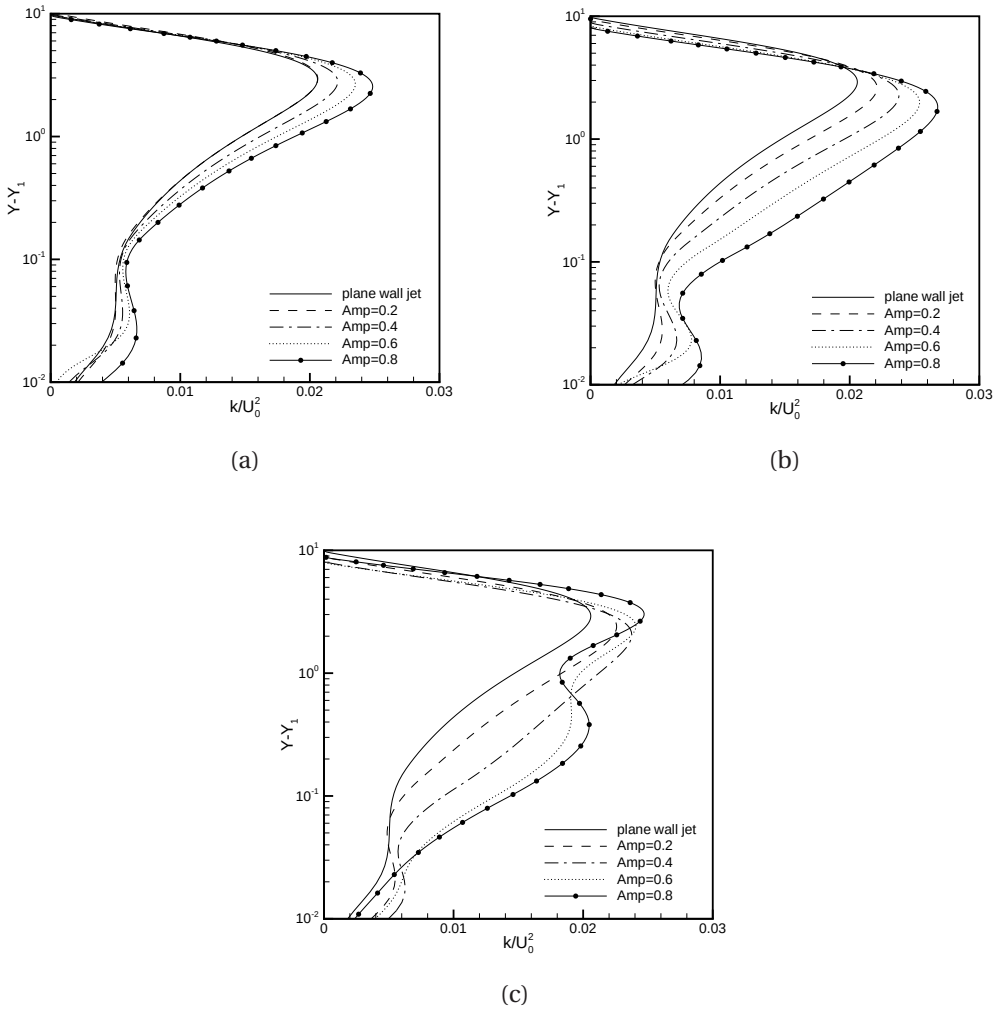

Figure 4.20: The variation of turbulent kinetic energy profile in cross stream direction for different amplitudes for (a) ω_4 at $X = 42.1875$(3rd crest), (b) ω_8 at $X = 39.8375$(5th crest) and (c) ω_{12} at $X = 39.0625$ (7th crest)

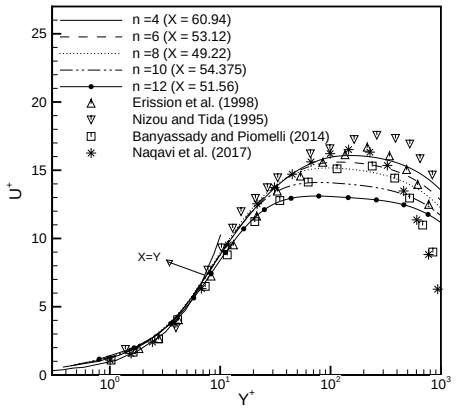

Figure 4.21: The variation in velocity profile near the wall at crest for different frequencies for amplitude 0.4

these two peaks the turbulent kinetic energy is minimum at the position of U_{max} as the velocity gradient (du/dy) becomes zero at this location. In the case of ω_{12}, for the amplitudes 0.6 and 0.8, the secondary peak is shifted upwards and this might be due to increase in the thickness of inner shear layer for 0.6 and 0.8 amplitudes (fig. 4.17c). The maximum jump in turbulent kinetic energy is 24%, 33.9% and 23.5% for frequency ω_4, ω_8 and ω_{12}, respectively with respect to the plane wall jet.

4.2.2.5 Velocity profile near the wall

The profiles of u^+ and y^+ are plotted in fig. 4.21 to get a clear picture of flow behavior near the wall. Fig. 4.21 shows the variation of velocity profile near the wall at the crests for different frequencies for amplitude 0.4. The results are compared with the results available in the literature [13, 25, 67, 71] for plane wall jet. The velocity profile for all the cases remains same till buffer layer and starts deviating in the logarithmic zone. As the frequency increases, the velocity u^+ starts reducing and the peak also gets flatten for ω_{10} and ω_{12}. The velocity profile for ω_4 is in a good agreement with the result of Eriksson et al. [25] and Naqavi et al. [67]. It can be seen from the fig. 4.21 that the velocity profile near the wall follows the universal law of wall relationship for all the frequencies. In the logarithmic zone, the profile follows the logarithmic relation $u^+ = C_1\, ln(y^+) + C_2$, where $C_1 = 2.3$ and C_2=5.8 for ω_4. The value is close to the plane wall jet results mentioned by Eriksson et al. [25] ($C_1 = 2.44$ and $C_2 = 5.0$) and Naqavi et al. [67] ($C_1 = 2.5$ and $C_2 = 5.2$). The constants of logarithmic relation for all the frequencies are listed in the table. 4.4. The constant C_1 decreases from 2.3 to 0.88 and constant C_2 increases from 5.8 to 9.5, as the frequency in-

Table 4.4: The change in logarithmic equation constant C_1 and C_2 in velocity profile for different frequency.

Frequency (ω_N)	C_1	C_2	R^2 (goodness of fit)	Range
ω_4	2.3	5.8	98.2%	$30 \leq y^+ \leq 90$
ω_6	1.75	7.9	96.1%	$30 \leq y^+ \leq 86$
ω_8	1.58	8.5	96.0%	$30 \leq y^+ \leq 70$
ω_{10}	1.12	8.6	95.6%	$30 \leq y^+ \leq 60$
ω_{12}	0.88	9.5	95.0%	$30 \leq y^+ \leq 57$

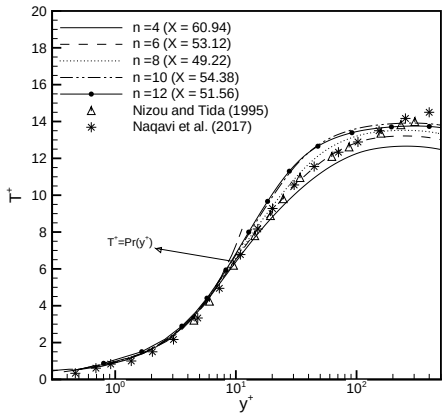

Figure 4.22: The variation in temperature profile near the wall at crest for different frequencies for amplitude 0.4.

creases from ω_4 to ω_{12}. The range for which the logarithmic equation is valid also reduces with the increase in frequency.

4.2.2.6 Temperature profile near the wall

The T^+ and $y+$ graphs are plotted to explain the temperature profile in the near wall region, just like u^+ and y^+ for the flow field. Fig. 4.22 shows the influence of frequency on the temperature profile near the wall at the crest for the amplitude 0.4 and the results are compared with the result of [67, 71]. The linear relation "$T^+ = Pr\, y^+$" is followed by all the cases up to $Y^+ = 7$. Nizou and Tida [71] have also noticed the same observation in their study. For n=4, the logarithmic relation constants for the range of $30 \leq y^+ \leq 90$ are $C_1 = 1.93$ and $C_2 = 3.5$ which are close to the result $C_1 = 2.08$ and $C_2 = 3.5$, as mentioned by Naqavi et al. [67]. The constants of the logarithmic equation for all the cases are listed in table. 4.5. The range of the logarithmic zone remains same for all the frequencies.

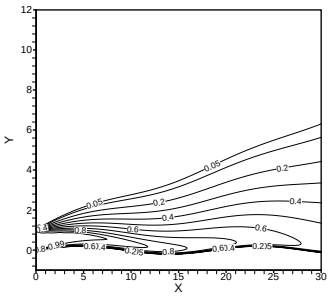

(a) A=0.2, ω_4

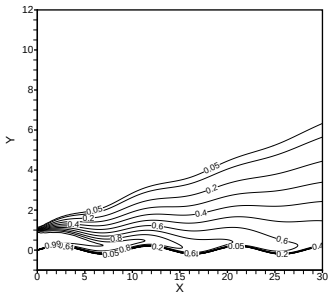

(b) A=0.2, ω_8

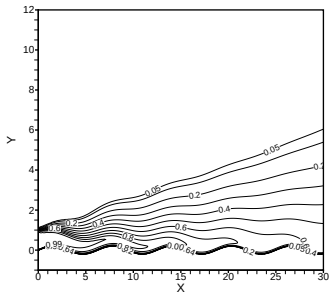

(c) A=0.2., ω_{12}

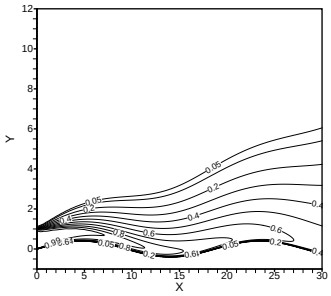

(d) A=0.4, ω_4

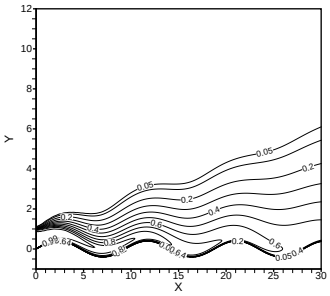

(e) A=0.4, ω_8

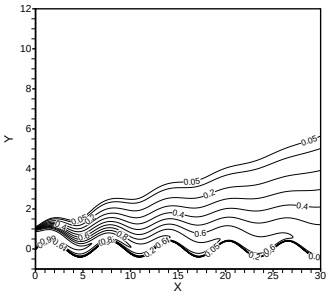

(f) A=0.4, ω_{12}

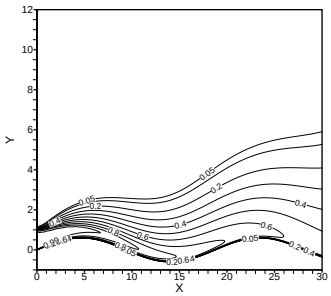

(g) A=0.6, ω_4

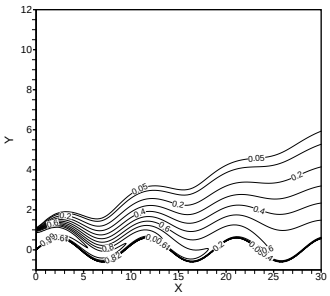

(h) A=0.6, ω_8

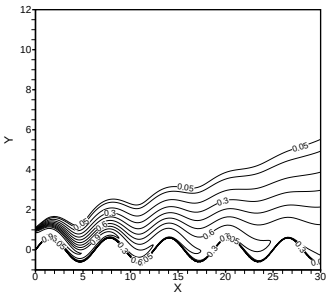

(i) A=0.6, ω_{12}

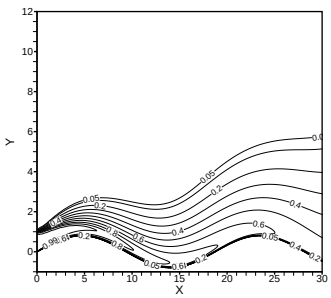

(j) A=0.8, ω_4

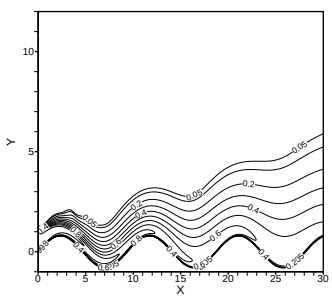

(k) A=0.8, ω_8

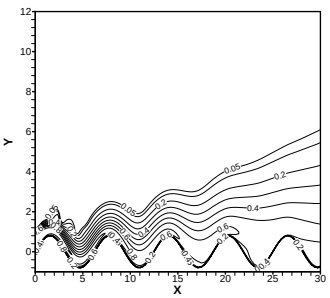

(l) A=0.8, ω_{12}

Figure 4.23: The temperature contour for different amplitudes and different frequencies

Table 4.5: The change in logarithmic equation constant C_1 and C_2 in velocity profile for different frequency

Frequency (ω_N)	C_1	C_2	R^2(goodness of fit)
ω_4	1.93	3.5	98.9%
ω_6	1.77	4.8	98.0%
ω_8	1.98	4.3	97.5%
ω_{10}	1.73	5.8	96.0%
ω_{12}	1.56	6.5	96.0%

4.2.2.7 Temperature contour

For the clear understanding of thermal distribution in the flow domain, the temperature contour is shown in fig. 4.23 for the amplitudes 0.2 to 0.8 and frequency ω_4, ω_8 and ω_{12}. As the frequency increases, the potential core becomes shorter and thinner, as shown in fig. 4.23. For ω_4, the potential core gets least affected by the increasing amplitude, i.e. potential core length reduces from $X = 7.2$ to $X = 6.1$ for A=0.2 to A=0.8 whereas potential core length decreased drastically from $X = 7$ to $X = 3.7$ for A=0.2 to A=0.8 for ω_{12}.

4.2.2.8 Local maximum temperature and thermal wall boundary layer

The influence of frequency and amplitude of sinusoidal wavy wall on the thermal characteristics is explained with the help of decay of normalized local maximum temperature $\theta_{max}$and the development of thermal wall boundary layer Y_{Tmax} in figs. 5.19a and 4.25, respectively. The fig. 5.19a shows the decay of local maximum temperature along the flow for different amplitudes and frequencies ω_4, ω_8 and ω_{12}. The results of Holland and Liburdy [41] and Rathore and Das [78] have been used for comparison with the present results. The Reynolds number used by [41, 77] is 15000, same as in the present work. The present result for the plane wall jet shows a good agreement with the experimental result of [41] along with a little deviation in the near field. Whereas the results of Rathore and Das [78] are slightly higher than the present result. The reason for this deviation is the difference in the methodology used. The conversion of thermal energy to the kinetic energy and increase in heat transfer to the bottom wall in the near flow field (discussed in fig. 5.8) lead to the reduction in thermal potential core length with the increasing amplitude as shown in fig. 5.19a. The decay of local maximum temperature also increases as the amplitude and frequency increase. In the far field, the decay of θ_{max} for all the cases becomes same as the decay of plane wall jet. The fig. 4.25 illustrates the effect of different amplitudes for the wavy wall with ω_4, ω_8 and ω_{12} frequency on the development of Y_{Tmax}. With the increase in amplitude the thermal wall boundary layer increases near the trough

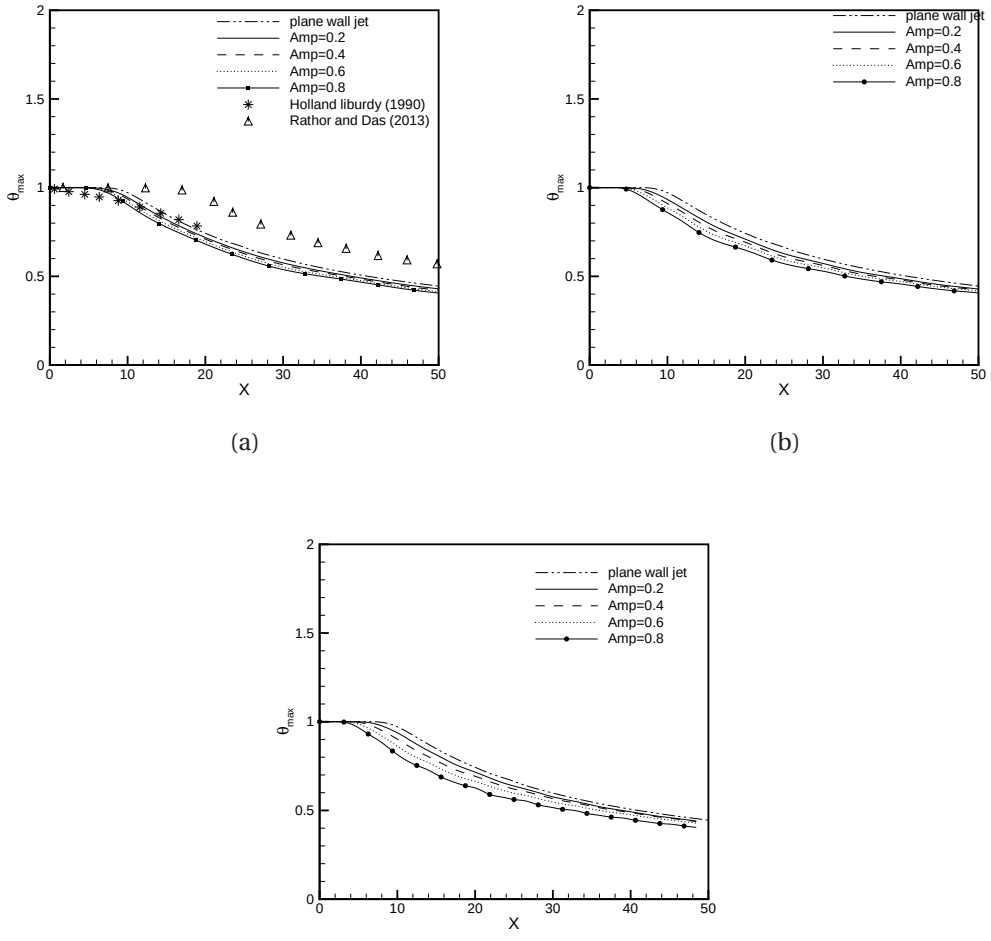

Figure 4.24: The variation of local maximum temperature for different amplitudes for (a) ω_4 ,(b) ω_8 and (c) ω_{12}

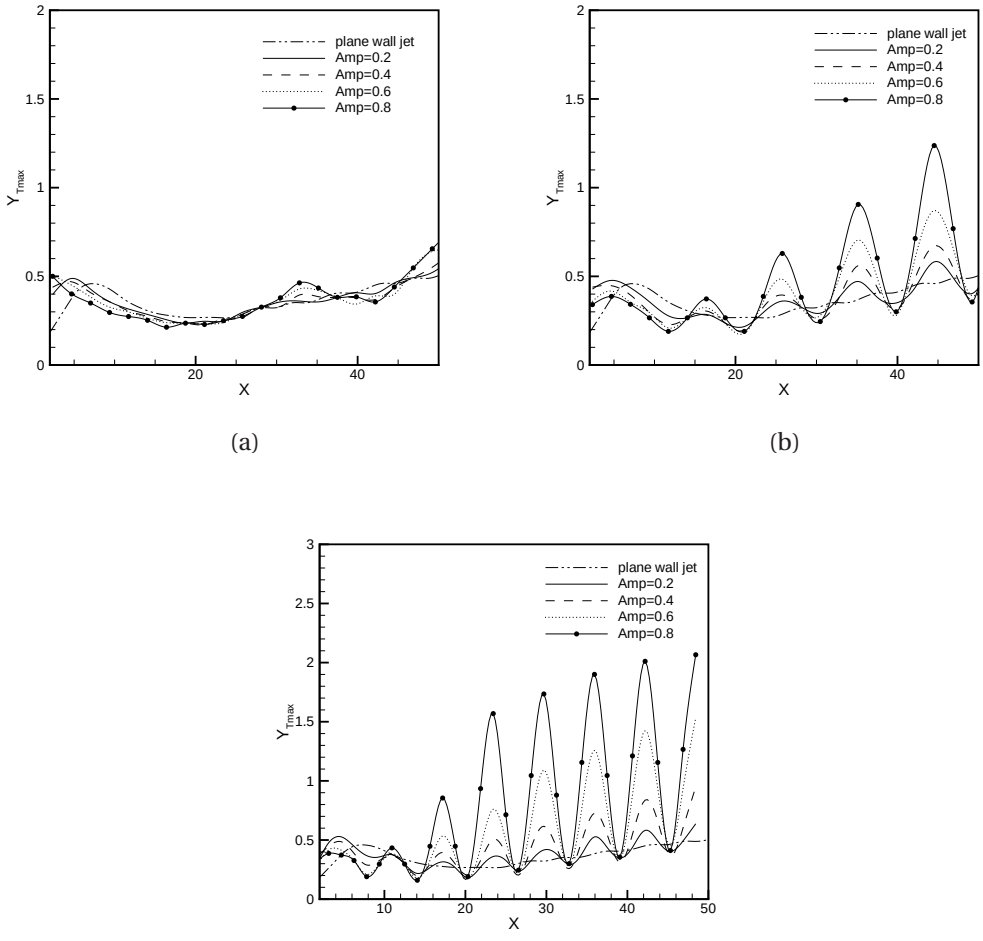

Figure 4.25: The variation of thermal wall boundary layer thickness for different amplitudes for (a) ω_4 ,(b) ω_8 and (c) ω_{12}

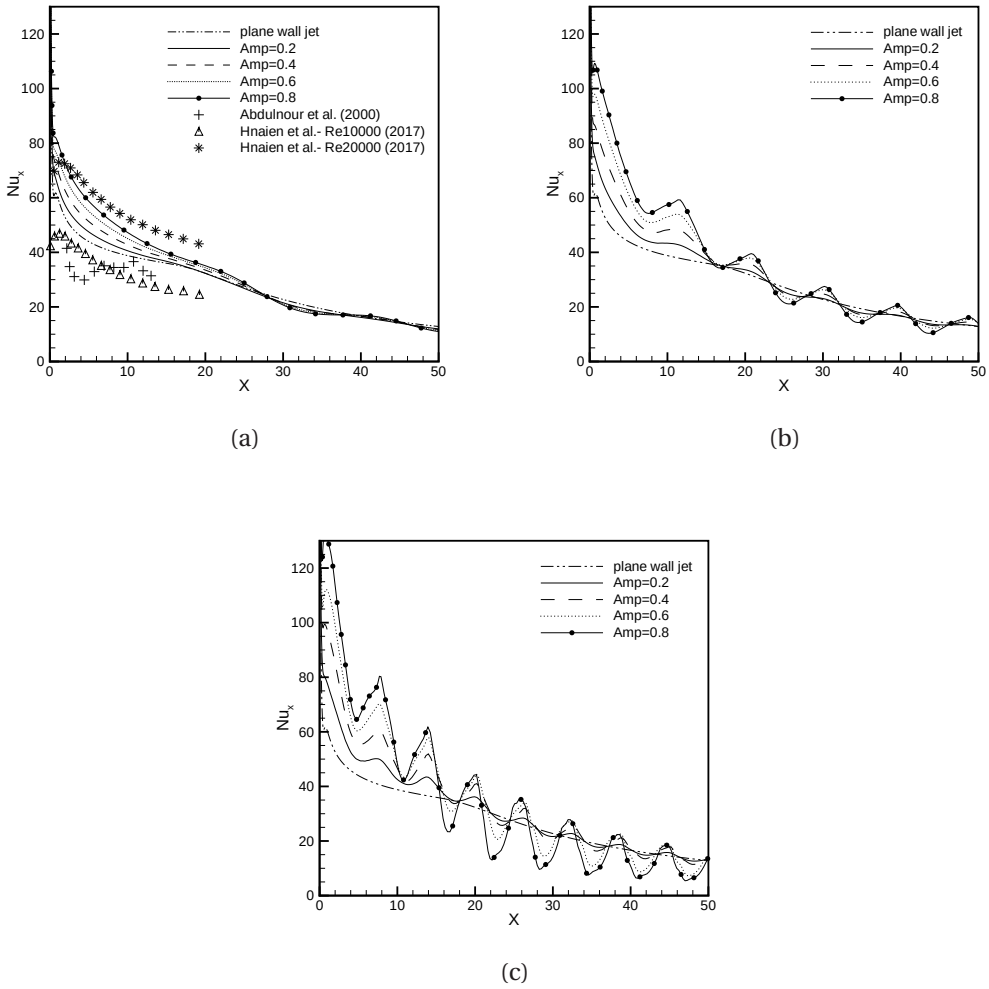

Figure 4.26: The variation of local Nusselt number on the wavy wall for different amplitudes for (a) ω_4 ,(b) ω_8 and (c) ω_{12}

region. However, a very marginal change is noticed at the crest. There is a similarity in the trend of Y_{Tmax} and the inner shear layer Y_{max}(fig. 4.17).

4.2.2.9 Nusselt Number

To study the effect of wavy wall on heat transfer rate, the trend of local Nusselt number is presented in fig. 5.8. The figs. 4.26a, 4.26b and 4.26c are the variation of Nu_x for different amplitudes of the wavy wall with frequency ω_4, ω_8 and ω_{12} respectively. The results are compared with the experimental result of AbdulNour et al. [1] and the numerical result of Hnaien et al. [38]. In the case of wavy surface, the local Nusselt number is higher in crest region and lower in the trough region because in the crest region, the momentum of flow

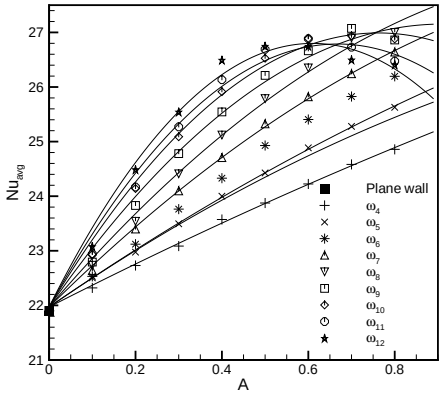

Figure 4.27: The trend of average Nusselt number for different amplitudes of frequency ω_4 to ω_{12}.

is high, however in trough region momentum reduces due to the expansion of flow. In the case of ω_4, ω_8 and ω_{12}, the Nu_x increases with the increasing amplitude in the near field till $X \leq 28$, $X = 23.5$ and $X = 15$ respectively. Beyond this location, the influence of amplitude becomes negligible for ω_4. However, in the case of ω_8 and ω_{12}, the Nu_x decreases for the higher amplitude and becomes even less than the plane wall near the trough region. The trend of average Nusselt number for each frequency against the amplitude is plotted in fig. 4.27. The average Nusselt number for the plane wall jet is also plotted for the reference. The average Nusselt number increases with the increasing amplitude up to ω_8; for $\omega_8 > 8$, the average Nusselt number starts decreasing for the higher amplitude. The maximum enhancement of 23.23% in heat transfer is noticed in comparison to the baseline case, for the wavy wall with frequency ω_9 and amplitude 0.7. Singh et al. [92] have mentioned a maximum increment of 14.43% for the wavy wall with a frequency ω_7 and amplitude 0.7 by using standard $k-\varepsilon$ model. Further increasing the amplitude and frequency increases the recirculation area drastically (mentioned in table. 4.3) which leads to the reduction in the heat transfer rate. The trend of Nu_{avg} for each frequency ω_4 to ω_{12} follows a quadratic relation with amplitudes as $Nu_{avg} = C_1 A^2 + C_2 A + 21.97$ for $A \leq 0.8$, where C_1, and C_2 are constants which are mentioned in table. 4.6. For each frequency, the quadratic relation has a goodness of fit more than 99% with the present data. The constant C_1 has negative sign and the magnitude of constants C_1, and C_2 are increasing with the increasing frequency of wavy wall.

Table 4.6: The constants for the quadratic equation followed by different frequency for average Nusselt number and amplitude.

Frequency (ω_N)	C_1	C_2
ω_4	-0.48	4.03
ω_5	-1.05	5.44
ω_6	-1.38	6.46
ω_7	-2.43	7.82
ω_8	-3.42	9.23
ω_9	-6.23	11.39
ω_{10}	-8.65	13.18
ω_{11}	-10.79	14.42
ω_{12}	-12.97	15.83

4.3 Conclusion

The effect of amplitude of wavy wall on the fluid flow and heat transfer characteristics has been analyzed in detail. Based on the present results, the following conclusions can be drawn:

- As the amplitude of wavy wall increases from 0.1 to 0.8, the jet spread and inner shear layer growth increase in far field region $X \geq 15$.
- The local maximum streamwise velocity also increases with an increase in the amplitude, although the trend remains wavy throughout the flow with maxima at the crest and minima at the trough. The U_{mas} is maximum at the first crest in all the cases. TheU_{max} value at the first crest is increased by 37%, 71%, 103% and 137% for amplitude 0.2, 0.4, 0.6 and 0.8 respectively, in comparison to the plane wall jet.
- The flow remains attached to the surface throughout the flow till 0.3 amplitude. Beyond that, as amplitude increases from 0.4 to 0.8, the flow starts getting separated.
- The length of the thermal potential core decreases from $X = 7.5$ to $X = 3.75$ for the plane wall to the wavy wall of amplitude 0.8. The amplitude also affects the thickness of potential core, i.e the thermal potential core becomes thinner for higher amplitude.
- The local maximum temperature decay increases with an increase in amplitude of wavy wall.
- The effect of amplitude on local Nusselt number is prominent up to $X = 19$. There is an increase in the average Nusselt number with the increasing amplitude till 0.7

and then it reduces with a further increase in the amplitude. For higher amplitude, separation and recirculation start dominating, which traps small amount of fluid within the zone and the contact of flowing fluid with the wall is disconnected which leads to decrease in heat transfer rate.

- The THP has been improved by 5.3% for the wavy wall of amplitude 0.8, which is sufficiently high and can be taken into consideration for future practical applications in heat transfer enhancement.

The of frequency of wavy wall on the fluid flow and heat transfer characteristics has been analyzed in detail. For this, the frequency has be varied from ω_4 to ω_{12} and the results are compared with the plane wall jet. On the basis of results and discussion, the following conclusions can be drawn:

- In the near flow field region, the local maximum streamwise velocity increases with the increasing frequency. At the first crest location, the maximum value of U_{max} is achieved. For amplitude 0.8 , highest increment is noticed, i.e 45.8%, 102% and 170.4% for frequency ω_4 , ω_8 and ω_{12} respectively, in comparison to the plane wall jet.

- The flow separation is initiated for the first time for frequency ω_6 for amplitude 0.8. Before that, the flow remains fully attached to the wall throughout the domain for all the amplitudes. The location at which separation is initiated for the first time moves towards the nozzle as the A and ω_N increase. The area under the re-circulation zone also keeps on increasing with the increasing A and ω_N and covers up to 58.2% of the total area for A=0.8 and ω_{12}.

- The range for which the velocity profile, near the wall region, follows the logarithmic law gets reduced from $30 \leq y^+ \leq 90$ to $30 \leq y^+ \leq 57$ for ω_4 and ω_{12}, respectively. Whereas the range of logarithmic law remains the same for all the frequencies in the case of temperature profile.

- The influence of amplitude on heat transfer rate is more prominent in the near flow field. The local Nusselt number increases with the increasing amplitude till the location $X = 28$, $X = 23.5$ and $X = 15$, for ω_4 , ω_8 and ω_{12} respectively. For ω_4, the influence of amplitude becomes negligible beyond $X = 28$. Whereas, the Nu_x starts decreasing for higher amplitudes and at the trough, the value even goes less than the value for the plane wall jet for frequency ω_8 and ω_{12}.

- For every frequency, the average Nusselt shows a quadratic relation with the amplitude. In comparison to the plane wall jet, the maximum heat transfer enhancement of 23.23% has been achieved for the wavy wall with ω_9 and A=0.7. Further increase in amplitude and frequency increases the re-circulation zone, which reduces the heat transfer rate.